Earthq Eng & Eng Vib (2008) 7:113-124 **DOI**: 10.1007/s11803-008-0831-x

Seismic vulnerability evaluation of axially loaded steel built-up laced members I: experimental results

Kangmin Lee[1†] and Michel Bruneau[2‡]

1. *Department of Architectural Engineering, Chungnam National University, Korea*
2. *Department of Civil, Structural, and Environmental Engineering, University at Buffalo, State University of New York, USA*

Abstract: An experimental program was initiated to investigate the seismic performance of built-up laced steel brace members. Quasi-static testing of twelve typical steel built-up laced member (BLM) specimens was conducted. These were designed to span a range of parameters typically encountered for such members based on findings from a survey of commonly used shapes and details that have been historically used. The specimens were subdivided into groups of three different cross-sectional shapes, namely built-up I-shape section, and built-up box shapes buckling about the *x* or the *y* axis. Within each group, global and local buckling slenderness ratios had either *kl/r* values of 60 or 120, and *b/t* ratios of 8 or 16. The specific inelastic cyclic behavior germane to each specimen, and general observations on overall member hysteretic behavior as a function of the considered parameters, are reported. A companion paper (Lee and Bruneau 2008) investigates this observed response against predictions from analytical models, and behavior in the perspective of system performance.

Keywords: quasi-static testing; built-up laced compression member; experimental program; brace

1 Introduction

A large number of structures with steel built-up laced bracing members have been built throughout the United States, many in zones of moderate to high seismicity. These members, consisting of rolled plates, channels, and angles riveted together to create shapes with open webs or sides, have typically been designed to resist wind forces, but not earthquakes. Such structural members, when located along the load path followed by seismically-induced forces, may buckle, yield, or suffer brittle fracture. However, seismic evaluation of structures having built-up laced members (BLMs) is difficult due to the limited knowledge on the cyclic inelastic behavior of these members.

Some testing of bridge-specific laced members has been conducted by other researchers. For example, Uang and Kleiser (1997) and Dameron *et al*. (1997) investigated the cyclic inelastic response of three half-scale specimens subjected to various load eccentricities, and indicated that compressive capacity of the laced specimens could be predicted reliably taking into account shearing effects of lacing and effective length factors. However, specimens exhibited limited ductility and less overstrength that usually observed for monolithic cross-sections. Dietrich and Itani (1999), in similar half-scale specimen tests, showed that the laced members could not reach the capacity predicted by the AISC LRFD Specifications (1999).

Up until now, research to date has been for a specific project or application; consequently, it is difficult to draw general conclusions from those studies. Knowledge on the cyclic inelastic performance of BLMs over a broader range of member and cross-section slenderness is needed to expand the available database of knowledge. To this end, based on representative details encountered in practice, an experimental program was devised whereby such braces of several cross-sectional shapes and geometric configurations were tested to ascertain the inelastic deformation capability of these critical elements, and thus provide a set of reference benchmarks to evaluate the seismic vulnerability of structures constructed with such steel BLMs.

This paper describes the range of responses and behavior observed from this experimental program for each specific specimen considered, and consolidates findings into a few general observations on member cyclic inelastic behavior for the broader range of parameters considered. A companion paper (Lee and Bruneau, 2008) investigated observed response against predictions from analytical models, and behavior in the

Correspondence to: Kangmin Lee, Department of Architectural Engineering, Chungnam National University, Daejeon, 305-764, Korea
Tel: +82-42-821-5625; Fax: +82-42-823-9467
E-mail: leekm@cnu.ac.kr
†Assistant Professor; ‡Director, MCEER, Professor

Supported by: Federal Highway Administration Under Grant No. DTFH61-98-C-00094
Received February 27, 2008; **Accepted** April 21; 2008

perspective of system performance.

2 Selection of parameters

Drawings were obtained for a few existing bridges having truss substructures with BLMs. Design provisions and steel design textbooks published at the time when laced compression members were being used, were also reviewed (Ketchum, 1920; Kunz, 1915), along with recent research work conducted for the major crossings in California (Uang and Kleiser, 1997 and Dietrich and Itani, 1999). This provided a range of parameters typically encountered for such members that could be extracted, including typical built-up member configurations and lacing geometry, typical *b/t* and *kl*/*r* ratios for the built-up members and their lacings, connection details, and other lacing characteristics. As a result of this work (and considering the limited resources available), research focused on investigating the impact of the *b/t* and *kl/r* ratios on member cyclic inelastic behavior, selected values ranging from 8 to 16 and from 60 to 120, respectively. These are the two parameters with the greatest impact on compressive strength, and have been observed to have the greatest variability from the collected data. Typical values obtained in this survey for selected bridges are overlaid to this considered range of values in Fig. 1. While some bridges' members were observed to have *b/t* ratios in excess of 16, it was decided to restrict testing to specimens having *b/t* values of 8 and 16 to allow a comparison of the cyclic performance of members with considerably different expectations in terms of local buckling behavior. Likewise, it was judged that testing braces with slenderness of *kl/r* of 60 and 120 would encompass the range of member slenderness observed in bridges, while allowing for comparisons of the cyclic inelastic behavior of members expected to have significantly different levels of inelastic buckling.

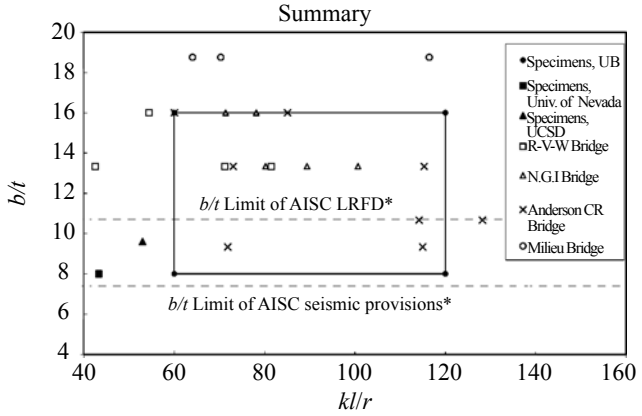

$$*b/t\,(\text{AISC LRFD}) = 200/\sqrt{F_y}\,(=76/\sqrt{F_y}) = 10.7, F_y = 345\text{MPa}\,(=50\text{ksi})$$

$$b/t\,(\text{AISC Seismic Provisions}) = 137/\sqrt{F_y}\,(=52/\sqrt{F_y}) = 7.4, F_y = 345\text{MPa}\,(=50\text{ksi})$$

Fig. 1 Distributions of *b/t* ratios and *kl/r* ratios

3 Overview of experimental program

3.1 Description of specimens

Three different types of cross-sections, again representative of data collected from existing bridges, were selected for this project. As shown in Fig. 2, specimens Ay were built using four angles, and specimens By and Bx using four angles and two tie plates. Cross-sections satisfying the target width-to-thick ratios, *b/t*, of 8 and 16, were built-up from angles 25×25×3.2 (1×1 ×1/8), 38×38×4.8 (1-1/2×1-1/2×3/16), and 51×51×3.2 (2×2×1/8). Lengths of the specimens and cross-section of the built-up shapes were then selected to provide the target slenderness ratios. Note that when calculating the cross-sectional properties of the specimens, the lacing members were not included, but the two tie-plates of the section shape of the "B" specimens were included. For the specimens with section shape "B", the direction of buckling was also controlled in the design by changing the width and depth of the test specimens. Note that the interest in testing section shape of the "B" specimens was to allow a comparison between different box-shaped members; in some cases, the lacing members would be in shear, and in others, they would not. Cross-sections for specimens with a *kl/r* of 60 and *kl/r* of 120 were identical for a given specimen name designation.

The resulting specimens designed based on the above considerations are presented in Fig. 2. Individual specimen names reflect the cross-section shape (A or B), the axis around which buckling may occur, and the *kl*/*r* and *b/t* values. Detailed drawings for specimens are presented in Lee and Bruneau (2004). Coupon tests for the steel used indicated the yield strength of 352 MPa for the angles, and 324 and 255 MPa for the 3.2 and 9.5 mm thick plates, respectively. Corresponding tensile strengths were approximately 483, 379 and 352 MPa, respectively.

3.2 Test set-ups and instrumentation

The test set-up is shown in Fig. 3 (Lee and Bruneau 2004). The original idea in designing the test set-up was that specimens having *kl/r* of 60 would be tested in an X-shape configuration, but with one of the braces not connected at its top end. This effectively made the braces with *kl/r* of 60 resist the tension and compression forces while the other brace in the X-braced configuration resisted no axial forces other than providing a bracing point at mid-length of the other member. The concept was then to remove the specimen having *kl/r* of 60 after it was tested, connect the top of the other brace, and test the second specimen having *kl/r* of 120 without having to change the configuration of the test set-up. However, this concept did not work as expected because it was not possible to fail and fracture the specimen having *kl/r* of 60 without introducing possible plastic deformations in the specimen having *kl*/*r* of 120. Therefore, to be able to test the specimen *kl/r* of 60 without introducing damage

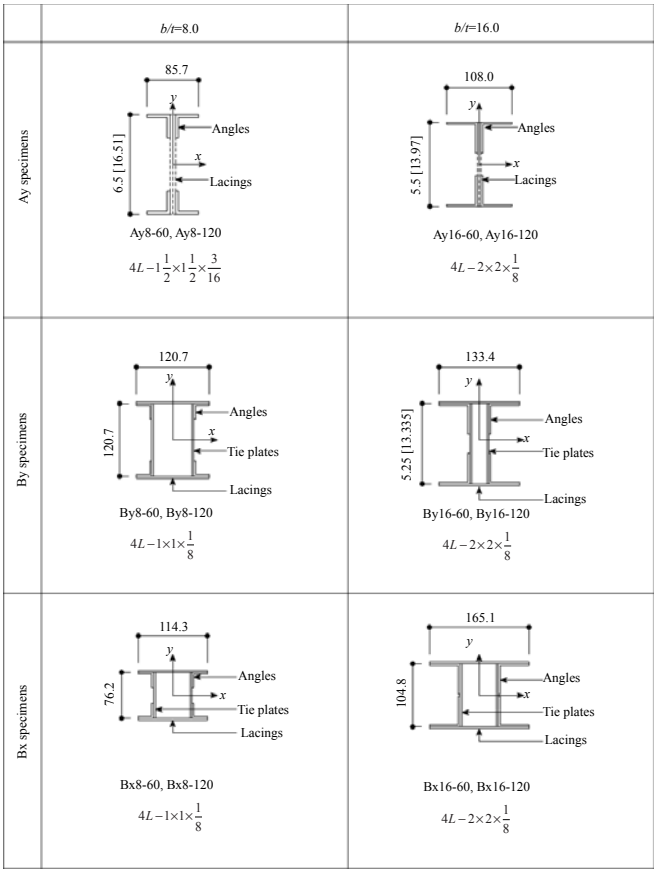

Fig. 2 Cross section shapes of the specimens (Length unit: mm)

in the other specimen, for all subsequent tests following the Ay8 series, dummy bracing members were used to provide the bracing point at the mid-length of the *kl/r* of 60 specimens. These dummy bracing members were designed to provide the same in-plane and out-of-plane flexural stiffness as would be encountered in the real X-braced frame configuration.

All specimens were instrumented with strain gauges to capture the brace axial and moment diagram (due to frame racking). The strain gauges were located at the 0.3 and 0.6 points of the center to center length of both the South and North segments of the specimens with *kl/r* of 60, and at the quarter and half points of the center to center length for specimens with *kl/r* of 120. Horizontal frame drift at the loading point and bottom of the frame was measured using Temposonic Magnetic Strictive Transducers (Temposonics). Temposonics were also used for measuring the axial displacement of the specimens (Lee and Bruneau, 2004).

4 Testing of specimens

4.1 Loading protocol

In all cyclic tests, the specimens were loaded by quasi-static cycles following the ATC 24 loading protocol (ATC, 1992), where specimens are subjected to three cycles at each prescribed displacement step up to three times the yield displacement, after which only two

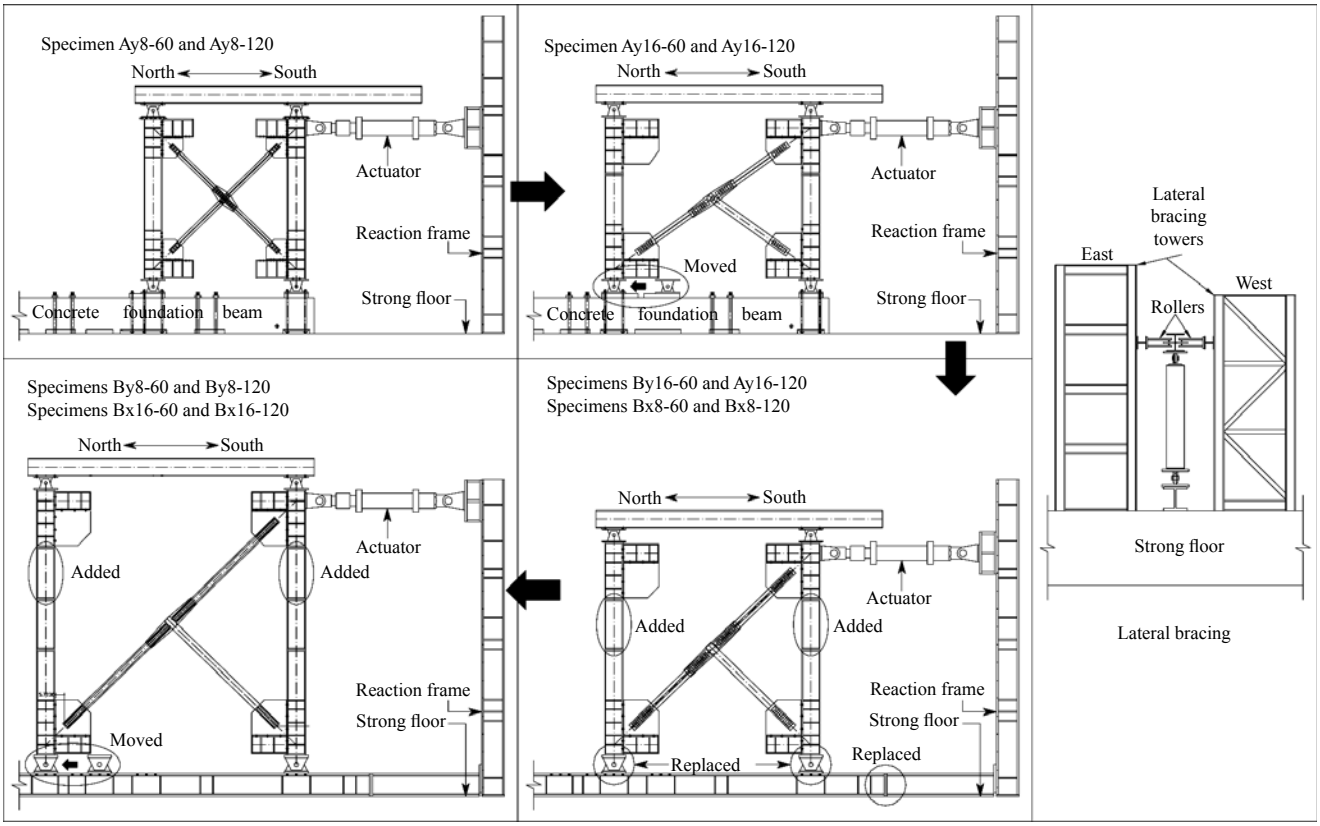

Fig. 3 Test set-ups and lateral bracing

cycles are necessary at each displacement target.

The difficulty in using the ATC 24 loading procedure lies in defining yield displacement before testing. Furthermore, because this paper focuses more on the compressive behavior of the laced built-up bracing member than on their tensile behavior, the experimentally determined displacement at the onset of buckling was substituted for the yield displacement in the ATC 24 protocol. Cycles of loading up to buckling were performed, then once the buckling displacement was identified experimentally, the subsequent cycles were done by controlling the displacement of the actuators.

5 Experimental observations

The experimental observations made during testing of the twelve specimens are presented in this section. The diagonal axial forces referred to in this section are converted from the horizontal forces applied by the hydraulic actuator, and diagonal axial displacements were directly measured by Temposonics displacement transducers installed diagonally. The hysteretic curves for three cross-section types (i.e., specimens Ay, By, and Bx), are presented in Figs. 4 to 6, respectively. The corresponding loading histories are shown in Figs. 7 to 9 to document the sequence of limit states reached throughout the cyclic testing. Note that the base hinges of specimens Ay were supported on a reinforced concrete foundation beam (contrary to the specimens By and Bx on a steel foundation beam).

5.1 Specimen Ay 8-60

Initial loading cycles applied to the specimens were based on their theoretically calculated elastic displacements, and the equivalent horizontal frame drift (Δ_b) at brace buckling was used to control the test. However, after six cycles at 1/3 Δ_b and 2/3 Δ_b (three cycles each) in the elastic range, strains from test results were compared with results from SAP 2000 analyses. Significant discrepancies were noted as the frame proved to be significantly more flexible as a consequence of excessive deformations in the concrete foundation beam and hinges. Because of these relatively large differences between theoretical and experimental results, a decision was made to seek the experimental buckling frame drift, $\Delta_{b,exp}$, by subjecting the specimen to progressively increasing small values of the control displacement, starting from the theoretical 2/3 Δ_b = 5.08 mm (corresponding to a diagonal brace displacement, δ, of 0.508 mm). This experimental buckling drift was identified during the first compressive displacement at Δ = 25.4 mm (δ = 2.54 mm). Global buckling was observed in both the South and North segments of the

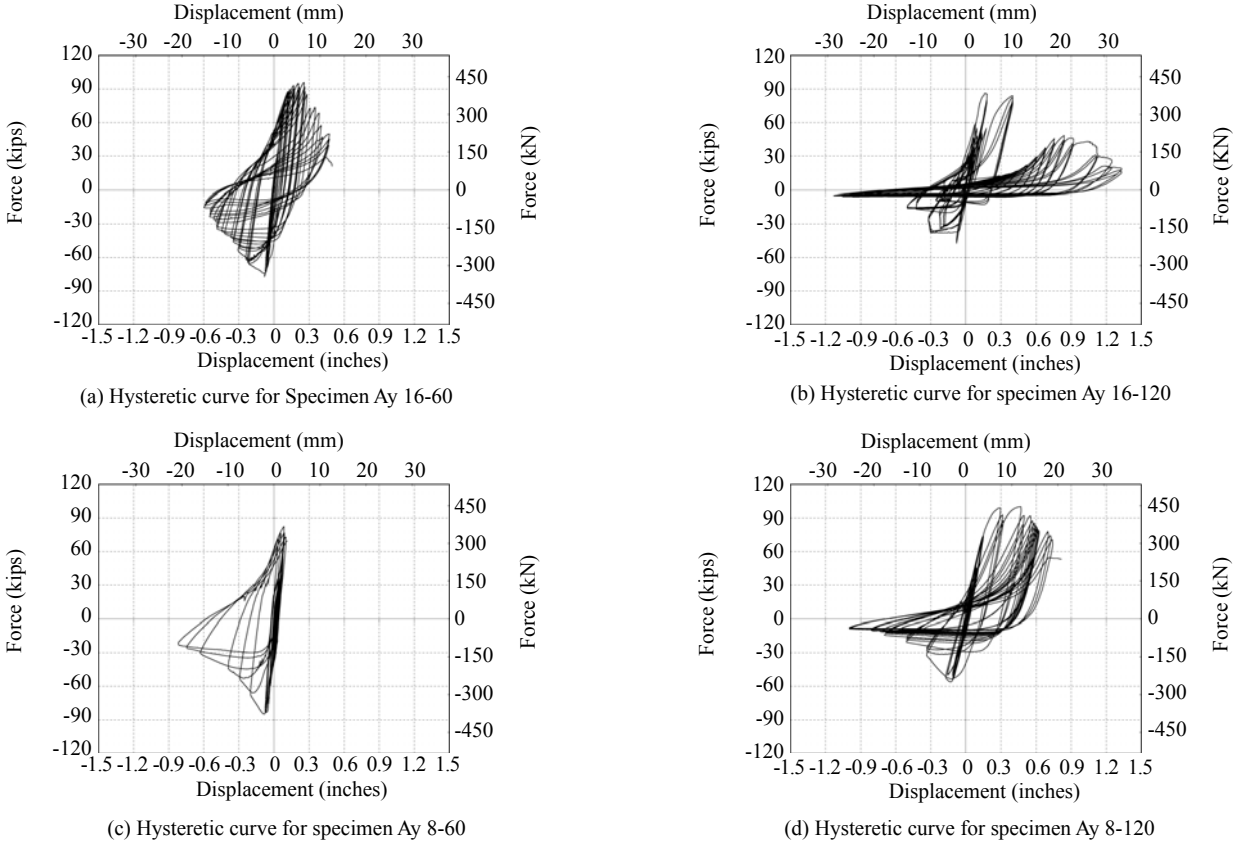

(a) Hysteretic curve for Specimen Ay 16-60

(b) Hysteretic curve for specimen Ay 16-120

(c) Hysteretic curve for specimen Ay 8-60

(d) Hysteretic curve for specimen Ay 8-120

Fig. 4 Hysteretic curves for Ay specimens

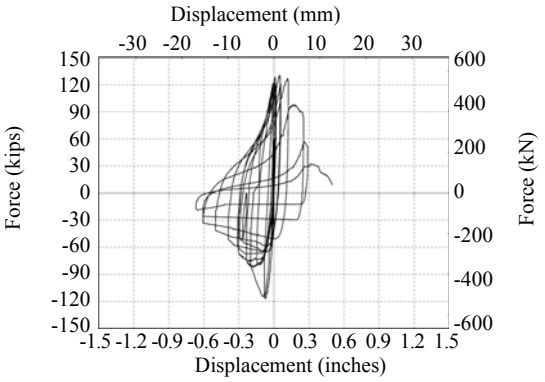

(a) Hysteretic curve for specimen By 16-60

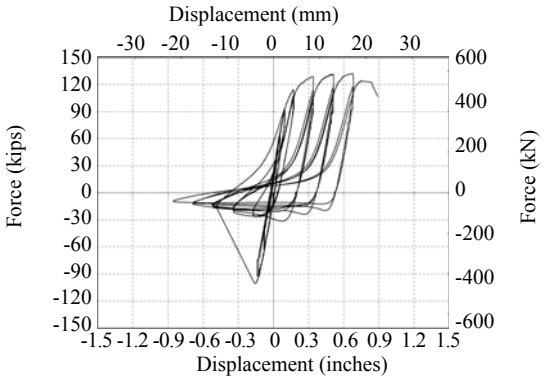

(b) Hysteretic curve for specimen By 16-120

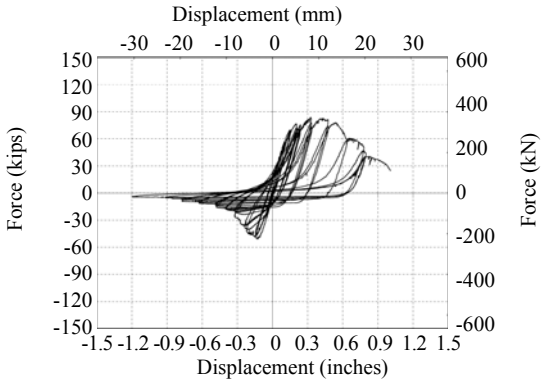

(c) Hysteretic curve for specimen By 8-60

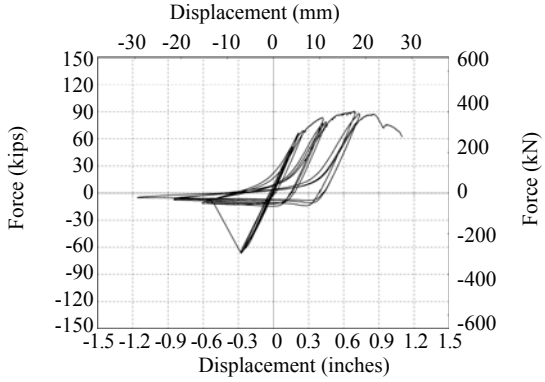

(d) Hysteretic curve for specimen By 8-120

Fig. 5 Hysteretic curves for specimens By

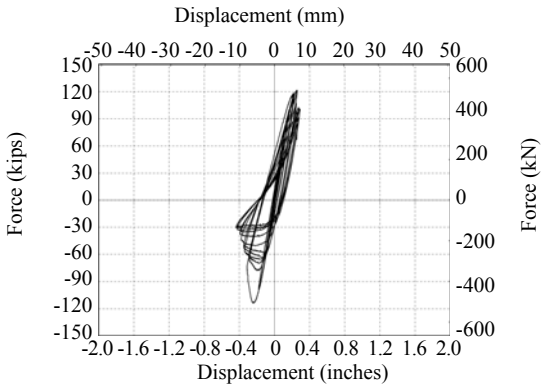

(a) Hysteretic curve for specimen Bx 16-60

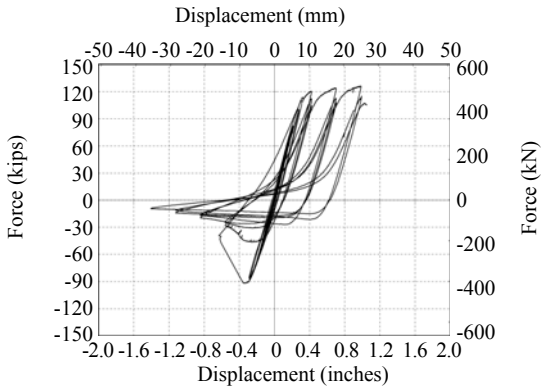

(b) Hysteretic curve for specimen Bx 16-120

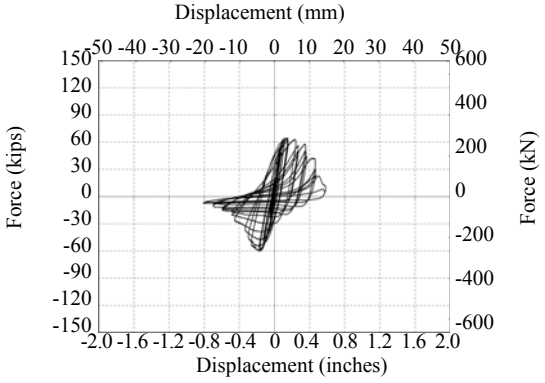

(c) Hysteretic curve for specimen Bx 8-60

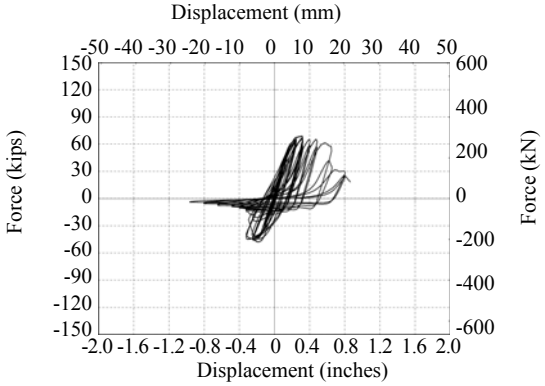

(d) Hysteretic curve for specimen Bx 8-120

Fig. 6 Hysteretic curves for specimens Bx

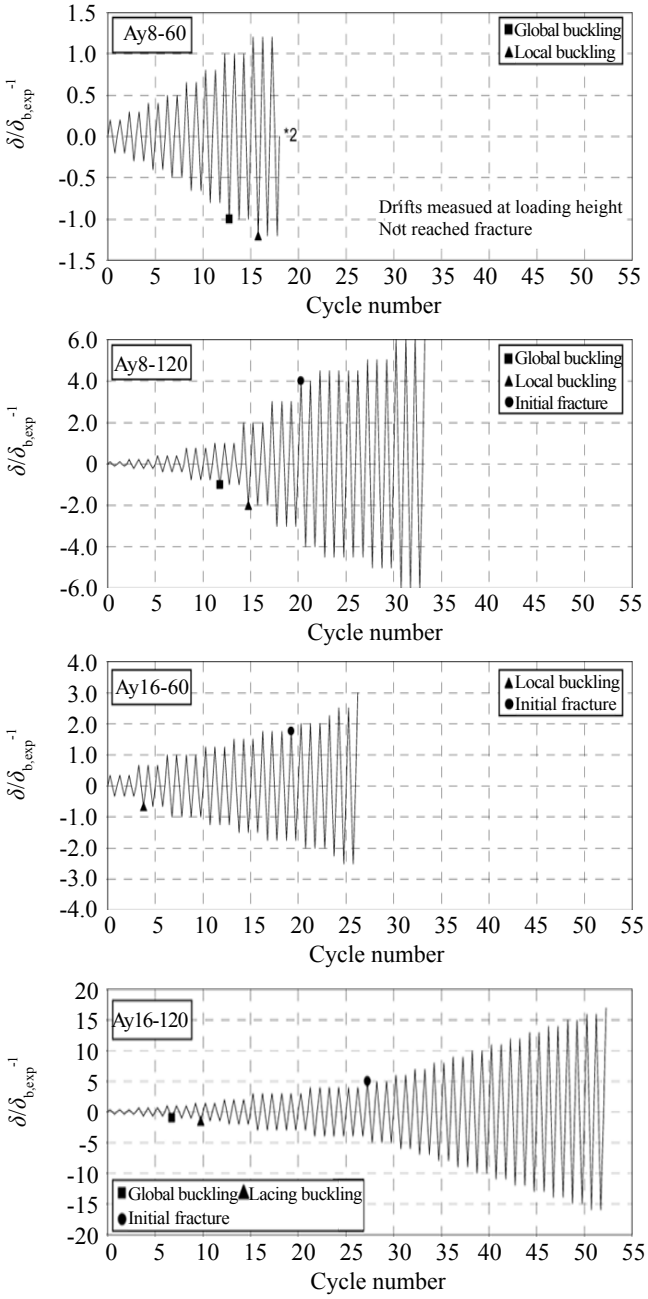

Fig. 7 Loading histories for specimens Ay

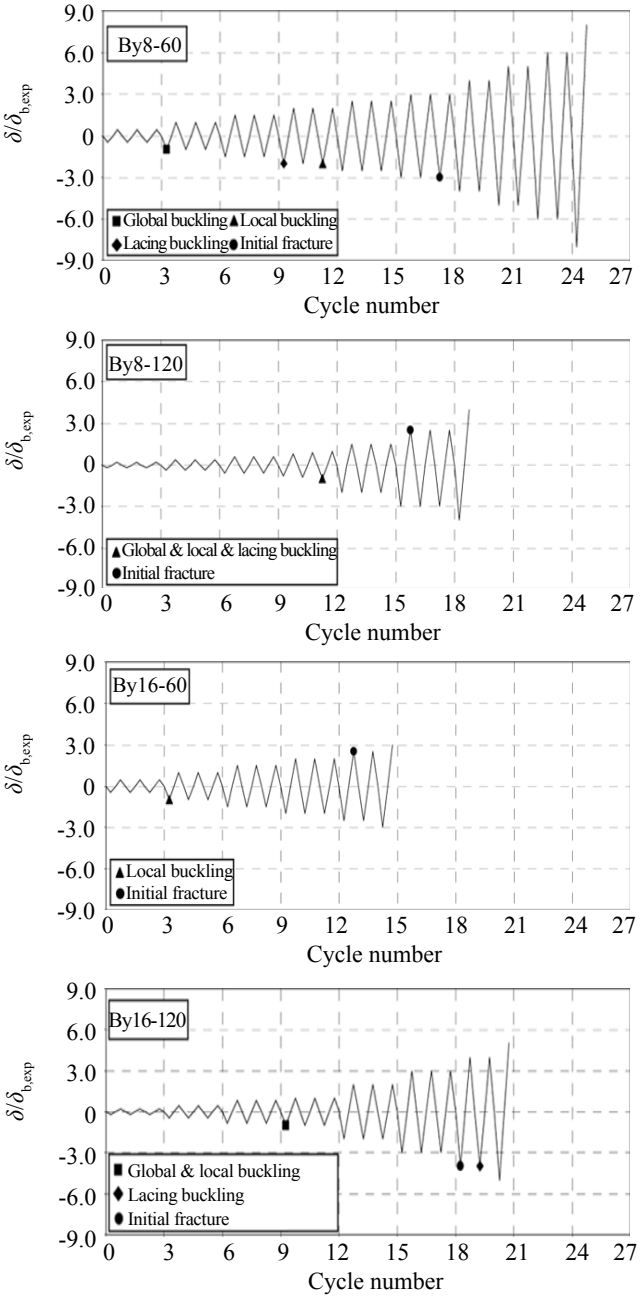

Fig. 8 Loading histories for specimens By

specimens. During visual inspection of the specimen after buckling, relatively small damage on the other diagonal specimen (Ay 8-120) was noticed. To prevent severe damage of the specimen Ay 8-120, testing was continued with a small increment of 5.08 mm of the control displacement, Δ.

During the first compressive cycle at Δ = 30.5 mm (δ = 16.0 mm), more severe global buckling was observed and local buckling was also observed on the angles at the plastic hinge locations at mid-length of both the South and North segments of the specimens. Although the specimen had not reached fracture, testing was stopped to prevent severe damage on the Ay8-120 specimen. Note that the compressive strength had dropped to about 1/3 of its maximum compressive force at that point.

Note that from this point forward, all subsequently tested specimens having *kl/r* of 60 were supplied with mid-length bracing as described in Section 3.2.

5.2 Specimen Ay 8-120

Testing of the Ay 8-120 specimen was controlled by diagonal axial displacements of the specimen instead of horizontal frame drifts, because movement in the hinges and in the concrete foundation beam made it too difficult to establish a reliable relationship between these two displacement measures and because the focus of this

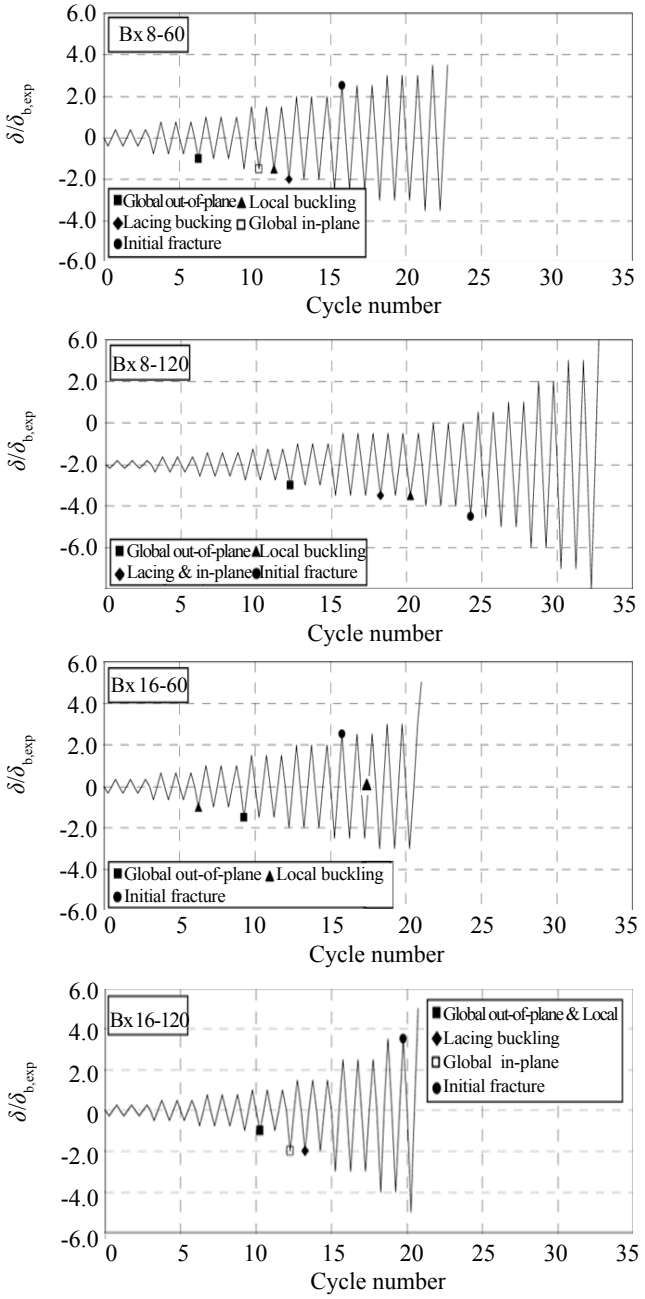

Fig. 9 Loading histories for specimens Bx

research project was more on the axial displacement behavior of the bracing member than on drifts of the braced frame.

The theoretically calculated elastic buckling displacement (δ_b) was used to control the displacements for the first set of testing cycles, but no evidence of buckling or yielding was observed after 12 cycles at 1/3 δ_b, 2/3 δ_b, 1.0 δ_b, and even 2.0 δ_b (3 cycles each). This was due to greater than expected flexibility of the specimen, as in all cases the corresponding applied axial brace force was less than the theoretically computed strength. During the first compressive cycle at 2.5 δ_b, global buckling at mid-length of the specimen was observed and the experimental buckling displacements, $\delta_{b,exp}$ = 4.1 mm were identified. This value was then used as the reference control displacement for continuous testing per the ATC-24 protocol.

During the first compressive cycle at 2.0 $\delta_{b,exp}$, both the larger global and local bucklings were observed, at the location of initial buckling and near the mid-length brace plastic hinge, respectively. During the first tensile cycle at 4.0 $\delta_{b,exp}$, initial fracture was observed on the upper angle at the global and local buckling location. Entire fracture of the specimen occurred at 6.0 $\delta_{b,exp}$ and the fractured shape is shown in Fig. 10.

5.3 Specimen Ay 16-60

Loading was controlled by diagonal axial displacement of the entire specimen, i.e., the cumulative displacement over both segments on each side of the mid-length brace. During the first compressive cycle at 1.0 δ_b = 5.59 mm, local buckling was observed on the upper angles near the middle connection plate on the North segment of the specimen and the experimental buckling displacement was identified as $\delta_{b,exp}$ = 5.59 mm. The corresponding experimental buckling displacements for each of the South and North segments of the specimen were identified as 2.79 mm. From that point, loading of the specimen proceeded on the assumption that damage would concentrate on the North segment, leaving the South segment intact. Therefore, smaller cyclic displacement steps should be applied using total member length as a control, to indirectly control the North segment displacements. Observations confirmed that buckling, damage, and inelastic deformation concentrated only on the buckled North segment.

As such, after the three cycles at 1.0 $\delta_{b,exp}$, three cycles at δ = 1.25 $\delta_{b,exp}$ were applied, which was assumed to correspond to 1.5 $\delta_{b,exp}$ of the North segment and 1.0 $\delta_{b,exp}$ of the South segment. The decision to apply 1.5 $\delta_{b,exp}$ on the North segment instead of 2.0 $\delta_{b,exp}$ was to allow better observations of other local buckling which might be missed if larger displacement increments were used.

During the third tensile cycle at δ = 1.75 $\delta_{b,exp}$ (2.5 $\delta_{b,exp}$ of the North and 1.0 $\delta_{b,exp}$ of the South segments),

Fig. 10 Fractured shape of specimen Ay 8-120

initial fracture was observed on the lower angle near the middle connection plate of the North segment of the specimen. During the first tensile cycle at δ = 3.0 $\delta_{b,exp}$ (5.0 $\delta_{b,exp}$ of North and 1.0 $\delta_{b,exp}$ of South specimen), entire fracture near the middle connection plate of the North segment was observed. Fig. 11 shows buckled shapes of Ay8-60 (global buckling governs) and Ay 16-60 (local buckling governs) specimens for comparison purposes.

5.4 Specimen Ay 16-120

During the first compressive cycle at 1.0 δ_b, global buckling was observed near the mid-length of the specimen and the experimental buckling displacements, $\delta_{b,exp}$ = 2.22 mm, were identified. During the first compressive cycle at 1.5 $\delta_{b,exp}$ (instead of 2.0 $\delta_{b,exp}$ for the same purpose as Specimen Ay16-60), larger global buckling was observed at the location of initial buckling and accompanied by local buckling on the lower angle near the mid-length brace plastic hinge location.

During the first tensile cycle at 5.0 $\delta_{b,exp}$, initial fracture was observed on the lower angle near the mid-length of the specimen and another local buckling was also observed on the upper angles near the North gusset-connection. At the loading cycles of 14.0 $\delta_{b,exp}$, maximum actuator stroke was reached in compression, and the control displacement increased only in tension (for example, 14.0 $\delta_{b,exp}$ in tension and 13.0 $\delta_{b,exp}$ in compression). During the first tensile cycle at 17.0 $\delta_{b,exp}$ in tension, an entire fracture near the mid-length of the specimen was observed. Local buckling and fractured shapes of the Ay16-120 are presented in Fig. 12. Note that some hysteretic curves during mid-test were lost due to a fault of the data acquisition system.

5.5 Specimen By 8-60

Before testing the By 8-60 specimen, the concrete foundation beam and hinges at the bottom of the frame were replaced with a steel foundation beam and better designed (slip-free) new hinges. This foundation beam was connected to the strong floor with a prestressed Diwidag bar to prevent slippage and lifting of the foundation beam. The revised set-up proved effective in preventing undesirable frame deformations due to movements in the foundation beam and hinges.

For all the section shape B specimens, testing was initially controlled relative to the lateral frame force, P_H, corresponding to the theoretical elastic brace buckling force until the experimental buckling displacements ($\delta_{b,exp}$) were identified. Beyond that point, subsequent

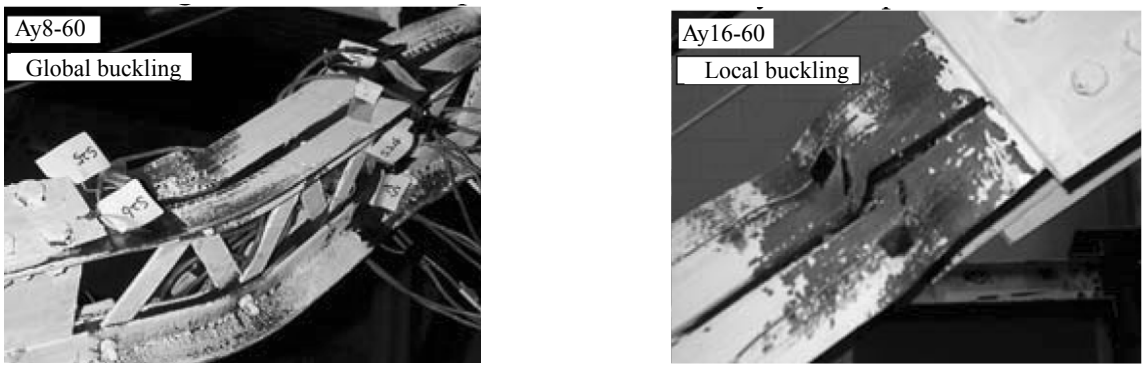

Fig. 11 Buckled shapes of specimens Ay 8-60 and Ay 16-60

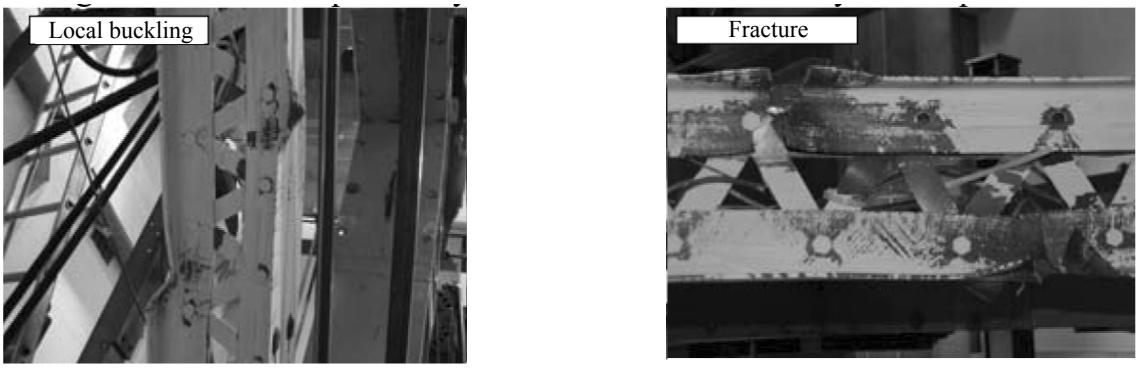

Fig. 12 Local buckling and fracture of specimen Ay16-120

cycles were controlled using target displacements.

During the first compressive cycle at 2/3 P_H = 160.2 kN corresponding to the 2/3 δ_b, the onset of global buckling was observed in the North segment of the specimen and the experimental buckling displacements, $\delta_{b,exp}$ = 3.6 mm, were identified. During the first compressive cycle on the way to the target value of 1.5 $\delta_{b,exp}$, global buckling occurred suddenly in the North segment of the specimen when the control displacement had only reached 4.3 mm. During the first compressive cycle at 2.0 $\delta_{b,exp}$, lacing buckling on the North segment was observed. Lacing buckling gradually spread to the locations of the North segment during the second and third cycles at 2.0 $\delta_{b,exp}$ as shown in Fig. 13. Lacing buckling caused the two channels that constituted the cross-section to move closer together, resulting in a smaller moment of inertia (I) for the specimen and consequently a greater drop in compression strength during compressive cycles. During the third compressive cycle at 3.0 $\delta_{b,exp}$, initial fracture was observed on the lower angle near the 5th lacing from the top of the North segment. During the first tensile cycle at 8.0 $\delta_{b,exp}$, entire fracture was observed at the initial fracture location.

5.6 Specimen By 8-120

Because no evidence of buckling or yielding was observed after nine cycles at the theoretical 1/3 P_H, 2/3 P_H, and 1.0 P_H (three cycles each), or even during the first cycle at 1 1/3 P_H = 178 kN, a small increased control force, starting from P_H = 186.9 kN to 204.7 kN for the third loading cycle was progressively applied to find the experimental buckling displacement. During the third compressive cycle at 204.7 kN, significant global buckling suddenly developed near mid-length of the specimen. In addition to local and lacing buckling, lacing bolt failure was observed near the global buckling location during this cycle and the experimental $\delta_{b,exp}$ = 7.1 mm was identified.

During the first tensile cycle at 3.0 $\delta_{b,exp}$ = 21.3 mm, initial fracture on the lower angle near the 7th lacing from the South end of the specimen was observed and entire fracture at this location developed at the first tensile cycle at 4.0 $\delta_{b,exp}$.

5.7 Specimen By 16-60

During the first compressive cycle at 2/3 P_H = 342.7 kN, local buckling on the upper angle near the middle connection plate and lower angles near the gusset-connection in the North segment of the specimen were observed and the corresponding experimental buckling displacement, $\delta_{b,exp}$ = 4.1 mm was identified. These local buckles became more severe during the following compressive loading cycles.

Three loading cycles at 1.5 $\delta_{b,exp}$ of the specimen were applied to better observe the local buckling. During the first compressive cycle at 1.5 $\delta_{b,exp}$, local buckling on the tie-plates near the gusset-connection in the North segment of the specimen was observed and during the second compressive cycle, local buckling on the plates was so severe that bolts on the adjacent deformed upper and lower tie-plates came in contact. Initial fracture was observed on the lower angle near the gusset-connection during the first compressive cycle at 2.5 $\delta_{b,exp}$ and during the first tensile cycle at 3.0 $\delta_{b,exp}$, entire fracture was observed at this location as shown in Fig. 14.

5.8 Specimen By 16-120

Because no evidence of buckling or yielding was observed after nine cycles at the theoretical 1/3, 2/3, and 1.0 P_H = 2647.0 kN, a decision was made to seek the experimental buckling displacement by increasing small values of the control force, starting from P_H = 311.5 kN. During the first cycle at P_H = 311.5 kN, global buckling suddenly developed near the mid-length of the specimen. This resulted in a significant overshoot beyond the control displacement that the controllers could not prevent. Local buckling was also observed at the global buckling location and near both the South and North gusset-connections and the experimental buckling displacement, $\delta_{b,exp}$ = 4.3 mm was identified. During the first compressive cycle at 4.0 $\delta_{b,exp}$ =17.3 mm, initial fracture on the lower angle at the mid-length of the specimen was observed. During the first tensile cycle

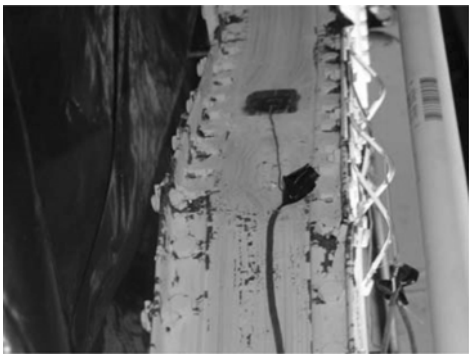

Fig. 13 Lacing buckling of specimen By 8-60

Fig. 14 Fractured shape of specimen By 16-60

at 6.0 $\delta_{b,exp}$, entire fracture of the lower angle at the mid-length of the specimen was observed.

5.9 Specimen Bx 8-60

During the first compressive cycle at 1.0 P_H = 387.2 kN, global buckling in the South segment of the specimen was observed and the experimental buckling displacements, $\delta_{b,exp}$ = 4.6 mm was identified.

During the first compressive cycle at 1.5 $\delta_{b,exp}$, global out-of-plane buckling was observed in the South segment as shown in Fig. 15. However, during the second compressive cycle, the out-of-plane buckling behavior permanently changed into an in-plane mode of buckling. This buckling axis change into in-plane was observed during subsequent testing of all the Bx specimens, which were originally designed to develop out-of-plane buckling. Lacing buckling and lacing bolt failure due to shearing effect, which was initiated with in-plane buckling, was observed during subsequent loading cycles. Initial fracture on the lower angle near the gusset-connection of the South segment of the specimen was observed during the first tensile cycle at 2.5 $\delta_{b,exp}$ and entire fracture near the middle connection plate of the South segment of the specimen was observed during the second tensile cycle at 3.5 $\delta_{b,exp}$.

5.10 Specimen Bx 8-120

Because no evidence of buckling or yielding was observed after nine cycles at the theoretical 1/3 P_H, 2/3 P_H, and 1.0 P_H (three cycles each), or even during three cycles at 1 1/3 P_H = 115.7 kN, a small increased control displacement, starting from 3.0 mm, which corresponds to the 1 1/3 P_H = 115.7 kN, was progressively applied to find the experimental buckling displacement. Initial global out-of-plane buckling was observed at the control displacement, δ_b = 4.1 mm, and the experimental buckling displacements, $\delta_{b,exp}$ = 4.1 mm, was identified.

Both out-of-plane and in-plane buckling were observed during the first compressive cycle at 1.5 $\delta_{b,exp}$ and lacing bolting failure was also observed near the North gusset-connection of the specimen. At the maximum displacement of the first compressive cycle at 2.0 $\delta_{b,exp}$, out-of-plane buckling behavior again permanently converted into in-plane buckling. During the first compressive cycle at 2.5 $\delta_{b,exp}$, initial fracture on the upper angle was observed at the mid-length of the specimen. During the second tensile cycle at 4.0 $\delta_{b,exp}$, fracture on the upper plate at mid-length of the specimen was observed, simultaneously with a large drop in tension strength. During the first tensile cycle at 6.0 $\delta_{b,exp}$ = 24.4 mm, the specimen fractured entirely at its mid-length.

5.11 Specimen Bx 16-60

After the first compressive cycle at 1.0 P_b = 293.7 kN, the force–displacement hysteretic curve that was monitored during the test showed some evidence of nonlinear behavior. No clearly visible local buckling was observed, but subsequent test cycles indeed proved that local buckling developed at the experimental buckling displacements, $\delta_{b,exp}$ = 5.1 mm corresponding to this load value.

During the first compressive cycle at 1.5 $\delta_{b,exp}$, large global out-of-plane buckling was observed in the South segment of the specimen. With this large global out-of-plane buckling, several areas of local buckling were observed: i) on the upper angles near the global buckling location, ii) on the lower angles of the South segment near the middle connection plate, iii) on the lower angle of the South segment near the gusset-connection, and iv) on the lower angles of the North segment of the specimen near the middle connection plate. During the first tensile cycle at 2.5 $\delta_{b,exp}$, fracture on the lower angle of the South segment near the middle connection plate was observed and propagated significantly during the second and third tensile cycles. During the third tensile cycle at 3.0 $\delta_{b,exp}$, entire fracture on the initial fractured location was observed.

5.12 Specimen Bx 16-120

No evidence of buckling or yielding was observed after nine cycles at the theoretical 1/3 P_H, 2/3 P_H, and 1.0 P_H = 240.3 kN. To find the experimental buckling displacement, the control force was progressively

Fig. 15 Out-of-plane buckling of specimen Bx 8-60

Fig. 16 In-plane buckling of specimen Bx 16-120

increased, starting from 1 1/3 P_b = 320.4 kN. During the second compressive cycle at 1 1/3 P_b, local buckling on the lower angle near the South gusset-connection was observed. Again, buckling was somewhat sudden, resulting in an overshoot of the target displacement. Small but visible global out-of-plane buckling was also observed and corresponding experimental buckling displacements, $\delta_{b,exp}$ = 7.1 mm were identified.

Three cycles at 1.5 $\delta_{b,exp}$ in tension and 2.0 $\delta_{b,exp}$ in compression of the specimen (i.e., unsymmetrical control displacements) were applied to prevent unexpected fracture during the following tensile cycle before significant buckling could be observed in compression. During the first compressive cycle at 2.0 $\delta_{b,exp}$, local buckling on the upper angle near the South gusset-connection was observed at δ_b = 7.1 mm and larger global in-plane buckling was observed at δ_b = 14.2 mm as shown in Fig. 16. During the second tensile cycle at 4.0 $\delta_{b,exp}$, initial fracture on the lower angle at the global buckling location and during the first tensile cycle, entire fracture was observed at this location.

6 General observations

The governing buckling mode for specimens with larger *kl/r* and smaller *b/t* ratios was found to be global buckling, and for specimens with smaller *kl/r* and larger *b/t* ratios local buckling, as expected. Specimens with both larger *kl/r* and *b/t* ratios (specimens Ay 16-120, By 16-120, and Bx 16-120) initially buckled globally; however local buckling occurred not only at the plastic hinge location (i.e., initial global or local buckling location) but also at other unexpected locations primarily during the compressive cycles after the initial global buckling.

Specimens originally designed to buckle out-of-plane of the testing frame (i.e., specimens Bx series) initially showed out-of-plane buckling during the first few elastic cycles, but this behavior permanently converted into in-plane buckling after the maximum buckling forces were reached.

The shape of the hysteretic curves for axially loaded built-up specimens having section shape B and larger *kl/r* (i.e., By 8-120, By 16-120, Bx 8-120, Bx 16-120) was similar to that of monolithic compression members before the lacing buckling. Note that no lacing buckling was observed for the section shape A and section shape B with both smaller *kl/r* and *b/t* specimens (i.e., By 16-60 and Bx 16-60 specimens). Once lacing buckling occurred, it led to a significant drop in compression strength due to the reduction in the sections' moment of inertia that resulted when the connected angles moved closer to each other.

Sudden global buckling was observed for all section shape B specimens with *kl/r* of 120 except Bx 8-120. This sudden and relatively large buckling was accompanied by lacing and local buckling, resulting in a significant strength degradation during the subsequent compressive loading cycles. Again, this was primarily due to the reduced moment of inertia caused by lacing buckling of the specimen.

Generally, specimens with section shape "A" (i.e., forming I shape) experienced larger inelastic deformation than specimens with section shape "B" (i.e., forming box shape). Specimens with both larger slenderness and width-to-thickness ratios experienced larger inelastic axial deformation than specimens with smaller slenderness and larger width-to-thickness ratios. The performance of specimens with larger slenderness ratios and smaller width-to-thickness ratios was between these two.

7 Conclusions

Twelve steel built-up laced members (BLMs) with I-section shapes (labeled "Ay"), or boxed shapes (labeled "By" when buckling about the *y* axis, or "Bx" about the *x* axis) were subjected to quasi-static cyclic axial loads. The specimens were chosen to have either *b/t* ratios of 80 or 120 and *kl/r* ratios of 60 or 120. All specimens were loaded until fracture of the members following ATC 24 loading protocol.

The BLMs with both smaller *kl/r* ratio and *b/t* ratio exhibited relatively "narrow" hysteretic curves, regardless of their section shapes, resulting in both smaller energy dissipation capacity and ductility capacity. Overall, specimens with section shape "Bx" showed a relatively inferior hysteretic behavior, i.e., narrow hysteretic curves, when compared with specimens of the other section shapes, such as "Ay" and "By."

Built-up brace specimens with lacing members designed to meet the slenderness requirements of the AISC LRFD specifications eventually buckled (albeit at relatively large deformation of the built-up specimens) for the section shape "B" specimens having larger slenderness ratios, resulting in a relatively larger axial strength deterioration after global buckling when compared with typical monolithic bracing members.

Local buckling not only at the plastic hinge location (i.e., globally buckled location), but also at other arbitrary locations, developed in the built-up laced bracing members having both larger *kl/r* ratio and *b/t* ratio, i.e., specimens Ay 16-120, By 16-120, and Bx 16-120.

The experimental data generated by this research provides a well-documented set of quasi-static cyclic inelastic test results of typical steel BLMs. This data will be used in the companion paper (Lee and Bruneau, 2008) to assess seismic performance in terms of ductility capacity, energy dissipation capacity, and strength degradation after buckling.

Acknowledgements

This work was conducted at the University at Buffalo and was supported by the Federal Highway Administration under contract number DTFH61-98-C-00094 to the Multidisciplinary Center for Earthquake Engineering Research. However, any opinions, findings, conclusions, and/or recommendations presented in this paper are those of the authors and do not necessarily reflect the views of the sponsors.

References

American Institute of Steel Constructions, Inc. (1999), *Load and Resistance Factor Design Specification for Structural Steel Buildings*, AISC, Chicago, Illinois.

Applied Technology Council (1992), "Guidelines for Cyclic Seismic Testing of Components of Steel Structures", *Report No. ATC-24*, ATC, Redwood City, California.

ASTM (1997), *Standard Specification for Commercial Steel Sheet, Carbon, Cold-Rolled*, *A 366/A 336M-97*, American Society for Testing and Materials, Philadelphia, Pennsylvania.

Dameron RA, Maxwell JS and Dunham RS (1997), "Pre-test Analysis of Three UCSD Laced Member Tests and Laced Member Modeling Recommendations," *Report* to Caltrans Laced Member Research Project Team, September, ANATECH, San Diego, California.

Dietrich Adrianne M and Itani Ahmad M (1999), "Cyclic Behavior of Built-up and Perforated Steel Members on the San Francisco–Oakland Bay Bridge," *Report No. CCEER 99-9*, June, Center for Civil Engineering Earthquake Research, University of Nevada, Reno, Nevada.

Ketchum Milo Smith (1920), *The Design of Highway Bridges of Steel, Timber and Concrete*, McGraw-Hill Co., New York, New York.

Kunz FC (1915), *Design of Steel Bridges; Theory and Practice for Use of Civil Engineers and Students*, McGraw-Hill Co., New York, New York.

Lee K and Bruneau M (2004), "Seismic Vulnerability Evaluation of Axially Loaded Steel Built-up Laced Members," *Report No. MCEER-04-0007*, June, Multidisciplinary Center for Earthquake Engineering Research, State University of New York, Buffalo, New York.

Lee K and Bruneau M (2008), Seismic Vulnerability Evaluation of Axially Loaded Steel Built-up Laced Members II: Evaluations," *Earthquake Engineering and Engineering Vibration*, **7**(2): 125-136.

Uang Chia-Ming and Kleiser Michael (1997), "Cyclic Performance of As-built Latticed Members for the San Francisco-Oakland Bay Bridge," *Report No. SSRP-97/01*, June, Division of Structural Engineering, University of California, San Diego, La Jolla, California.